Relative Permeability Correlation for Mixed-Wet Reservoirs

A. Kjosavik and **J.K. Ringen,** Statoil, and **S.M. Skjaeveland,** Stavanger U. College

Summary

A two-phase relative permeability correlation for mixed-wet rock is presented and validated. It includes provisions for bounding drainage and imbibition processes and scanning hysteresis loops, and is inferred from a capillary pressure correlation.

The well-known Corey-Burdine relative permeabilities were developed for water-wet rock from a Brooks-Corey power-law capillary pressure correlation and a bundle-of-tubes network model. We have extended this correlation to mixed-wet rock and now propose the ensuing relative permeability correlation for mixed-wet reservoirs. The functional form is symmetric with respect to fluid-dependent properties, because neither fluid has precedence in a mixed-wet environment. It reverts to the standard Corey-Burdine correlation for the completely water- or oil-wet cases, and exhibits the following characteristics in agreement with reported experiments: first, water-wet behavior at low water saturations and oil-wet behavior at low oil saturations; second, an inverted S-shape oil relative permeability curve with an inflection point; and, third, closed hysteresis scanning loops.

Introduction

Earlier,[1] we presented a capillary pressure correlation for mixed-wet reservoirs and suggested an extension of the Corey-Burdine[2,3] relative permeability relationship from water-wet to mixed-wet conditions. We now develop this idea further and include hysteresis logic. The main design constraints are:

- The functional form is symmetric with respect to oil and water. That is, the functional form is invariant to interchange of subscript *o* with subscript *w*.
- The hysteresis loops are closed.[4]
- The hysteresis loops of the capillary pressure and the relative permeabilities form a consistent set.[5,6]
- Imbibition oil relative permeability curves may exhibit a characteristic inverted "S" shape.[7–13]
- The validity of the relative permeability correlation and the hysteresis scheme is tested on published relative permeability measurements[4] and simultaneously measured hysteretic relative permeability and capillary pressure curves.[5] The hysteresis scheme is easy to program and could replace the Killough[14] scheme in numerical reservoir simulators.
- There is wide acceptance of the view that most reservoirs are mixed-wet, and network models[15] allow for this fact. However, to incorporate mixed-wet rock properties into a numerical reservoir flow simulator, validated correlations are required.[16–18]

Review of Capillary Pressure Correlation

The relative permeability correlation is inferred from the capillary pressure correlation,[1] and a review is given here. A sketch of the capillary pressure curve correlation for mixed-wet rock is shown in **Fig. 1**. It is an extension of the Brooks and Corey[19,20] correlation for primary drainage of a completely water-wet reservoir, which may be written as

$$p_{cd} = \frac{c_{wd}}{\left(\frac{S_w - S_{wR}}{1 - S_{wR}}\right)^{a_{wd}}}, \quad \ldots\ldots\ldots\ldots\ldots\ldots\ldots\ldots\ldots\ldots (1)$$

where c_{wd} = the entry pressure, $1/a_{wd}$ = the pore size distribution index,[2] and S_{wR} = residual (or irreducible) water saturation.

For primary imbibition of a completely oil-wet rock (i.e., the process of reducing the oil saturation from $S_o = 1$), the capillary pressure may also be represented by Eq. 1, with subscript *w* replaced by *o*. For the intermediate cases, the capillary pressure correlation is the sum of the two extremes

$$p_c = \frac{c_w}{\left(\frac{S_w - S_{wR}}{1 - S_{wR}}\right)^{a_w}} + \frac{c_o}{\left(\frac{S_o - S_{oR}}{1 - S_{oR}}\right)^{a_o}}, \quad \ldots\ldots\ldots\ldots\ldots\ldots\ldots\ldots\ldots\ldots (2)$$

where a_w, a_o, and c_w = positive constants, while c_o = a negative constant. There is one set of constants for imbibition and another for drainage. We use the term "drainage" if S_w is decreasing, and "imbibition" if S_w is increasing, irrespective of wettability preference.

Hysteresis Loop Logic. The design constraints follow from experimental evidence[21–26]:

- A saturation reversal on the primary drainage curve, before reaching the residual water saturation S_{wR} **(Fig. 2),** spawns an imbibition scanning curve aiming at a residual oil saturation determined by Land's trapping relation.
- Reversal from the primary drainage curve at S_{wR} starts an imbibition scanning curve down to S_{oR}. This curve is labeled (b) in Fig. 1 and is the bounding imbibition curve.
- The secondary drainage curve, labeled (c) in Fig. 1, is defined by a reversal from the bounding imbibition curve at S_{oR}. Together, the bounding imbibition and the secondary (bounding) drainage curves constitute the closed bounding hysteresis loop.
- All drainage scanning curves that emerge from the bounding imbibition curve scan back to S_{wR} **(Fig. 3),** and all reversals from the bounding drainage curve scan to S_{oR} **(Fig. 4).**
- A scanning curve originating from $S_w[j]$, the *j*'th reversal saturation, will trace back to $S_w[j-1]$ and form a closed scanning loop, unless a new reversal occurs.
- If a scanning curve tracing back from $S_w[j]$ reaches $S_w[j-1]$ before any new reversal (i.e., forms a closed scanning loop), the process shunts to the path of the $[j-2]$ reversal as if the $[j-1]$ reversal had not occurred, **Fig. 5.**
- The shape of a scanning loop is similar to the bounding loop because the *a* and *c* parameters are constants for a given rock-fluid system.

All properties of the *j*'th scanning curve are labeled by [*j*]. The capillary pressure is denoted by $p_{c\alpha}[j]$, where α denotes the process type and is either *i* for imbibition or *d* for drainage. By convention, *j* is an odd number for imbibition and even number for drainage, 0 denoting the primary drainage process. The asymptotes of the scanning curves are denoted by $S_{wR}[j]$ and $S_{oR}[j]$, and the water reversal saturation is denoted by $S_w[j]$. The smallest, "global" residual saturations of the largest bounding hysteresis loop are denoted by S_{wR} and S_{oR}.

All scanning curves are modeled by the same constants *a* and *c* as the bounding curves. As an example of the notation, the primary drainage capillary pressure is denoted by $p_{cd}[0]$, and its value at the first reversal, $S_w[1]$, is given by $p_{cd}[0](S_w[1])$.

First Reversal. A saturation process history of the fluid-rock system is required to enter the hysteresis loop system. We will assume that the rock initially is completely water-saturated. The first process will then be primary drainage. A reversal from primary drainage spawns an imbibition scanning curve $p_{ci}[1]$, scanning toward $S_{oR}[1]$. At the point of saturation reversal, $S_w[1]$, the

This paper (SPE 77328) was revised for publication from paper SPE 59314, first presented at the 2000 SPE/DOE Improved Oil Recovery Symposium, Tulsa, 3–5 April. Original manuscript received for review 13 April 2000. Revised manuscript received 2 July 2001. Manuscript peer approved 11 July 2001.

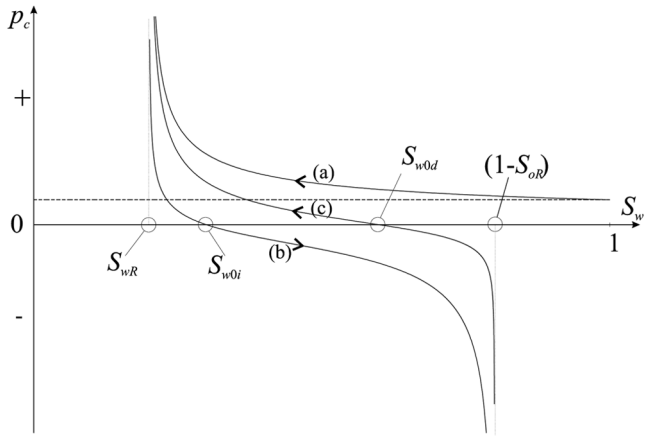

Fig. 1—Capillary pressure curves for (a) primary drainage, (b) bounding imbibition, and (c) secondary drainage.

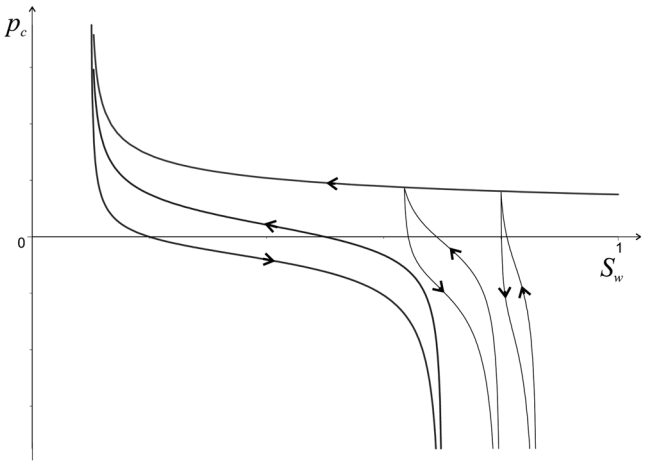

Fig. 2—Capillary-pressure scanning curves originating on the primary drainage curve.

imbibition scanning capillary pressure curve is equal to that of the primary drainage curve

$$p_{ci}[1](S_w[1]) = p_{cd}[0](S_w[1]), \quad \ldots\ldots\ldots\ldots\ldots\ldots\ldots\ldots (3)$$

where $p_{cd}[0](S_w[1])$ is given by

$$p_{cd}[0](S_w[1]) = \frac{c_{wd}}{\left(\frac{S_w[1] - S_{wR}}{1 - S_{wR}}\right)^{a_{wd}}}, \quad \ldots\ldots\ldots\ldots\ldots\ldots\ldots\ldots (4)$$

and $p_{ci}[1](S_w[1])$ by

$$p_{ci}[1](S_w[1]) = \frac{c_{wi}}{\left(\frac{S_w[1] - S_{wR}[1]}{1 - S_{wR}[1]}\right)^{a_{wi}}} + \frac{c_{oi}}{\left(\frac{S_o[1] - S_{oR}[1]}{1 - S_{oR}[1]}\right)^{a_{oi}}}. \quad \ldots\ldots (5)$$

To satisfy Eq. 3, we adjust the "water asymptote" $S_{wR}[1]$ and let the scanning curve aim at the "oil asymptote" $S_{oR}[1]$, determined by Land's equation

$$\frac{1}{S_{or}[1]} - \frac{1}{S_o[1]} = C, \quad \ldots\ldots\ldots\ldots\ldots\ldots\ldots\ldots\ldots\ldots (6)$$

where C = Land's trapping constant of the porous medium, and $S_o[1] = 1 - S_w[1]$. In the limit, if the first reversal from the primary drainage curve starts at $S_w[1] = S_{wR}$, the imbibition scanning curve is identical to the bounding imbibition curve. Fig. 2 shows scanning curves originating at two different values of $S_w[1]$, as well as the bounding hysteresis loop where $S_w[1] = S_{wR}$.

Second Reversal. A reversal on the scanning imbibition curve $p_{ci}[1]$ at $S_w[2]$ initiates a scanning drainage capillary pressure curve $p_{cd}[2]$ back to $S_w[1]$ to form a closed loop. At the two reversal points, the capillary pressures of the two scanning curves are equal:

$$p_{cd}[2](S_w[1]) = p_{ci}[1](S_w[1]), \quad \ldots\ldots\ldots\ldots\ldots\ldots\ldots\ldots (7)$$

$$p_{cd}[2](S_w[2]) = p_{ci}[1](S_w[2]). \quad \ldots\ldots\ldots\ldots\ldots\ldots\ldots\ldots (8)$$

The reversal at $S_w[2]$ may occur for any saturation between $S_w[1]$ and $1\text{-}S_{oR}[1]$. The oil and water scanning curve asymptotes $S_{oR}[2]$ and $S_{wR}[2]$ are the two unknowns in Eqs. 7 and 8, which are solved iteratively. A few iterations suffice.

Third Reversal. The $p_{cd}[2]$-process scans from $S_w[2]$ back to $S_w[1]$. Any new reversal $S_w[3]$ occurring before $S_w[1]$ is reached initiates an imbibition process back to $S_w[2]$ again (i.e., $p_{ci}[3]$ is equal to $p_{cd}[2]$ at $S_w[3]$ and $S_w[2]$). If, however, $S_w[1]$ is reached without any new reversal, the process is shunted from a $p_{cd}[2]$-curve to a $p_{cd}[0]$-curve (i.e., up the primary drainage curve), and the process history is erased.

More Reversals. Fig. 5 shows details of a set of enclosing scanning loops inside the bounding hysteresis loop. The first reversal (not shown) took place on the primary drainage curve $p_{cd}[0]$ at the global residual water saturation S_{wR} (i.e., at $S_w[1] = S_{wR}$), initiating the bounding imbibition curve $p_{ci}[1]$, which in turn was reversed at $S_w[2] = 1 - S_{oR}$, at the global residual oil saturation, and the secondary (bounding) drainage curve $p_{cd}[2]$ was spawned. The scan from $S_w[2]$ back to $S_w[1]$ is now interrupted by the third reversal at $S_w[3]$, the first reversal point shown in the figure. The imbibition scan $p_{ci}[3]$ from $S_w[3]$ is aimed back at $S_w[2]$, but is interrupted at $S_w[4]$ with a drainage process $p_{cd}[4]$ that aims back

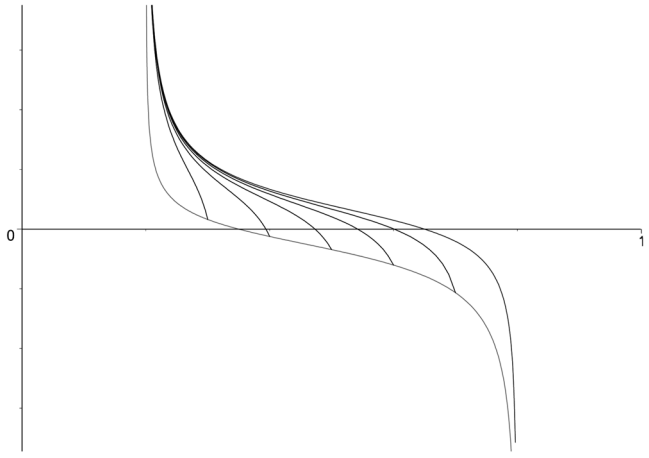

Fig. 3—Drainage capillary-pressure scanning curves originating on the bounding imbibition curve.

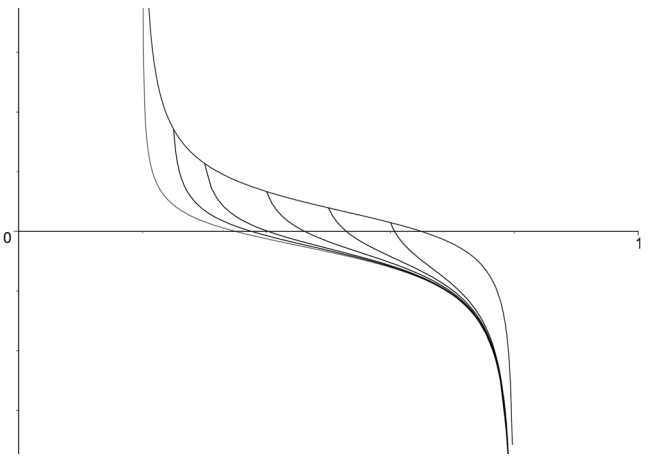

Fig. 4—Imbibition capillary-pressure scanning curves originating on the bounding drainage curve.

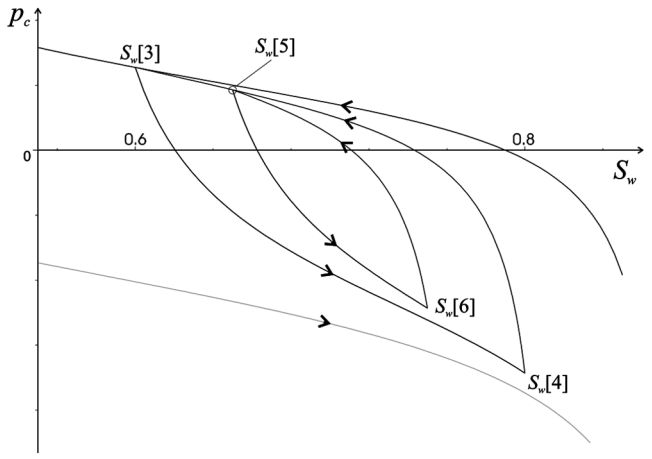

Fig. 5—Closed capillary-pressure scanning loops.

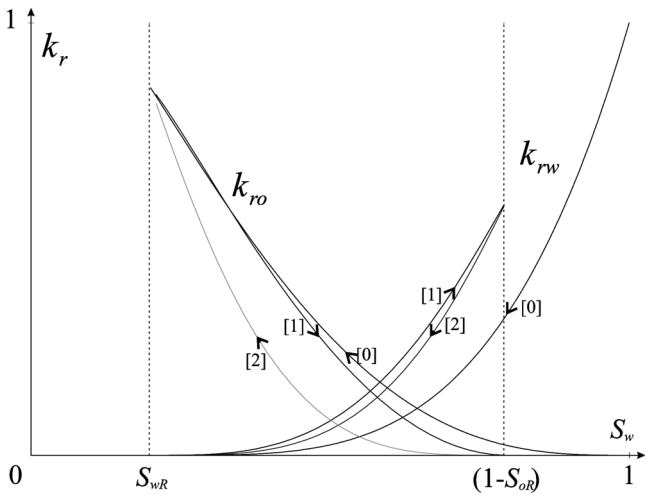

Fig. 6—Relative permeability curves for [0] primary drainage, [1] bounding imbibition, and [2] secondary (bounding) drainage.

at S_w[3]. Two more reversals occur, at S_w[5] and S_w[6]. From S_w[6], the drainage curve p_{cd}[6] scans back to S_w[5] and continues on the drainage process p_{cd}[4] to S_w[3]. Further drainage from S_w[3] follows the bounding drainage curve p_{cd}[2] back to S_{wR}, unless a new reversal occurs.

Relative Permeability Functions

We have developed a procedure similar to that of Corey and Burdine, reviewed in Ref. 27, to construct a relative permeability correlation for primary drainage and bounding drainage and imbibition curves for both oil and water, exemplified in **Fig. 6.** The development is based on Corey-type relative permeability functions, which are inferred from the Brooks and Corey capillary pressure correlation for water-wet porous medium, and the assumption of a bundle-of-tubes model for the pore network.

The general expression for capillary pressure, Eq. 2, consists of two Brooks-Corey type expressions (i.e., the water branch)

$$p_{cw} = \frac{c_w}{\left(\frac{S_w - S_{wR}}{1 - S_{wR}}\right)^{a_w}}, \quad \ldots\ldots\ldots\ldots\ldots\ldots\ldots\ldots\ldots\ldots (9)$$

and the oil branch

$$p_{co} = \frac{c_o}{\left(\frac{S_o - S_{oR}}{1 - S_{oR}}\right)^{a_o}}. \quad \ldots\ldots\ldots\ldots\ldots\ldots\ldots\ldots\ldots\ldots (10)$$

Each of these branches may now be combined with a Corey-Burdine integral over the capillary-tube size distribution[27] to render the wetting and nonwetting phase relative permeability functions. Note that the two branches in Eqs. 9 and 10 are valid for both drainage and imbibition, for four cases in all. When performing the integral over the capillary tubes, with the water branch for drainage and imbibition (i.e., with p_{cwd} and p_{cwi}), we get, in terms of the normalized saturations defined below,

$$k_{rw,wwd} = S_{nw}^{2a_{wd}+1+m_{wd}}, \text{ and } k_{rw,wwi} = S_{nw}^{2a_{wi}+1+m_{wi}} \quad \ldots\ldots\ldots\ldots (11)$$

for the relative permeabilities to water, with water as the wetting phase, and

$$k_{ro,wwd} = (1 - S_{nw}^{2a_{wd}+1})(1 - S_{nw})^{m_{od}},$$

$$k_{ro,wwi} = (1 - S_{nw}^{2a_{wi}+1})(1 - S_{nw})^{m_{oi}} \quad \ldots\ldots\ldots\ldots\ldots\ldots (12)$$

for the oil-relative permeabilities, with water as wetting phase.

If the same integration is performed with the oil branch for drainage and imbition (i.e., with p_{cod} and p_{coi}), we get

$$k_{rw,owd} = (1 - S_{no}^{2a_{od}+1})(1 - S_{no})^{m_{wd}},$$

$$k_{rw,owi} = (1 - S_{no}^{2a_{oi}+1})(1 - S_{no})^{m_{wi}} \quad \ldots\ldots\ldots\ldots\ldots\ldots (13)$$

for relative permeabilities to water in an oil-wet medium and

$$k_{ro,owd} = S_{no}^{2a_{od}+1+m_{od}}, \quad k_{ro,owi} = S_{no}^{2a_{oi}+1+m_{oi}} \quad \ldots\ldots\ldots\ldots\ldots\ldots (14)$$

for relative permeabilities to oil in an oil-wet medium. Here m_{wd}, m_{od}, m_{wi}, and m_{oi} are tortuosity exponents. Burdine[3] estimated a tortuosity exponent of 2.0 from experimental data. For primary drainage, $k_{rw,wwd}$ and $k_{ro,wwd}$ are used with $S_{oR} = 0$, and correspondingly for primary imbibition.

Normalized Saturations. The normalized saturations

$$S_{nw} = \frac{S_w - S_{wR}}{1 - S_{wR} - S_{oR}}, \quad \ldots\ldots\ldots\ldots\ldots\ldots\ldots\ldots\ldots\ldots (15)$$

and

$$S_{no} = \frac{1 - S_w - S_{oR}}{1 - S_{wR} - S_{oR}}, \quad \ldots\ldots\ldots\ldots\ldots\ldots\ldots\ldots\ldots\ldots (16)$$

in the relative permeability expressions, Eqs. 11 through 14, are different from the normalized saturations in the capillary pressure correlation (Eq. 2). However, the a-values are the same in both correlations, as can be seen by multiplying both the numerator and the denominator of the water branch term in Eq. 2 by

$$\left(\frac{1 - S_{wR}}{1 - S_{wR} - S_{oR}}\right)^{a_w}, \quad \ldots\ldots\ldots\ldots\ldots\ldots\ldots\ldots\ldots\ldots (17)$$

and the oil branch by

$$\left(\frac{1 - S_{oR}}{1 - S_{wR} - S_{oR}}\right)^{a_o}, \quad \ldots\ldots\ldots\ldots\ldots\ldots\ldots\ldots\ldots\ldots (18)$$

to render an adjusted Eq. 2 in the form

$$p_c = \frac{c'_w}{\left(\frac{S_w - S_{wR}}{1 - S_{wR} - S_{oR}}\right)^{a_w}} + \frac{c'_o}{\left(\frac{S_o - S_{oR}}{1 - S_{oR} - S_{wR}}\right)^{a_o}} \quad \ldots\ldots\ldots\ldots (19)$$

with c_w redefined to c'_w by

$$c'_w = c_w \cdot \left(\frac{1 - S_{wR}}{1 - S_{wR} - S_{oR}}\right)^{a_w} \quad \ldots\ldots\ldots\ldots\ldots\ldots\ldots (20)$$

and, correspondingly,

$$c'_o = c_o \cdot \left(\frac{1 - S_{oR}}{1 - S_{wR} - S_{oR}}\right)^{a_o}. \quad \ldots\ldots\ldots\ldots\ldots\ldots\ldots (21)$$

Tortuosity Exponent. With all tortuosity exponents m equal to 2, as offered by Burdine, the Corey-type relative permeability expressions are strictly monotonic functions of saturation; they have no inflection points. Several researchers[4,7,10,25,28–30] have ob-

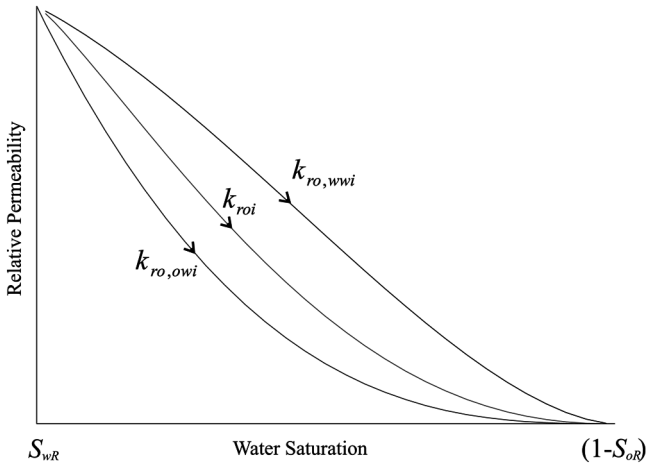

Fig. 7—Limiting oil-imbibition relative-permeability curves and resulting mixed-wet relative permeability k_{roi}.

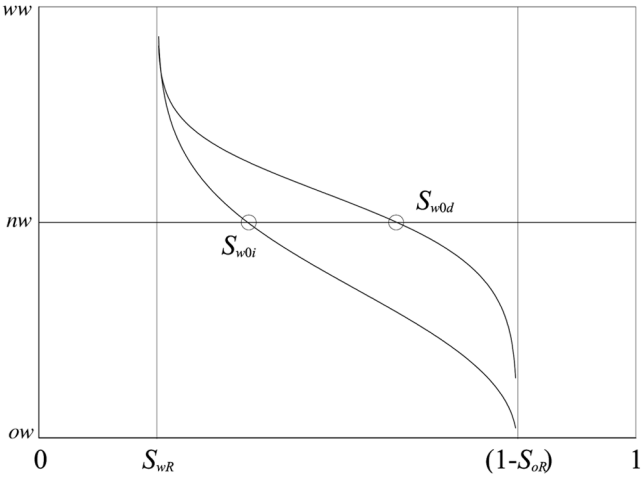

Fig. 8—Example of wettability functions; *ww:* water-wet; *nw:* neutral-wet; *ow:* oil-wet.

served, however, inverted S-shape oil relative permeability curves with an inflection point, especially for the bounding oil imbibition curve if oil is the nonwetting phase. There is almost no hysteresis in the wetting-phase properties.

Most of the measurements indicate that the bounding oil drainage curve lies below the bounding oil imbibition curve.[4,10,25,29,30] Illustrations by Honarpour[31] and measurements by Eikje *et al.,*[32] however, indicate the opposite behavior. To allow for both possibilities and the inverted S-shape curve, we introduce the tortuosity exponent m as a generalization of the Burdine[3] empirical tortuosity exponent of 2.0. Burdine introduced this parameter to compensate for the fact that the porous medium is not a bundle of straight, noninteracting capillary tubes. We will use four tortuosity exponents: m_{wd} and m_{od} for drainage and m_{wi} and m_{oi} for imbibition.

Mixed Wettability. The relative permeability expressions, Eqs. 11 through 14, are for the limiting wettability states (i.e., completely oil-wet or completely water-wet). In a mixed-wet system, each phase moves partly as a wetting phase and partly as a nonwetting phase. Therefore, the expression for mixed wettability should be symmetric. That is, if subscript w is swapped with o, the functional form should remain the same (i.e., the oil relative permeability function should look the same whether oil is considered to be wetting or nonwetting). Weighted summation of Eqs. 12 and 14 is consistent with a concept of parallel coupling of the oil-wetting and the water-wetting parts of the mobility of each phase. The weighting scheme should reflect the wettability state, and it seems reasonable that the mixed-wettability curve is between the two limiting curves, as in **Fig. 7** for the imbibition case.

Weighting With p_c. Earlier[1] we proposed to weight the limiting relative permeability expressions by the c-parameters in Eq. 2. This procedure presupposes constant wettability, independent of saturation. However, the wettability probably varies with pore radius and, therefore, saturation. A thinner water film in a pore will enhance adsorption of surface-active agents and make the pore more oil-wet.[12] The weight function imposes a continuous change in wettability with saturation–a gradual change from water-wet conditions in the smaller pore channels to oil-wet behavior in the larger pores. For example, water imbibing from S_{wR} will invade the small, water-wet pores and give a relative permeability change as for a water-wet system. At the other end, near S_{oR}, the relative permeability curves should vary as for a completely oil-wet medium. Such a wettability-dependent weighting of the water relative permeability functions, Eqs. 11 and 13, may be achieved by using the respective water and oil branches of the capillary pressure function, Eqs. 9 and 10, to give

$$k_{rwd} = \frac{p_{cwd}k_{rw,wwd} - p_{cod}k_{rw,owd}}{p_{cwd} - p_{cod}} \quad \ldots\ldots\ldots\ldots\ldots\ldots\ldots\ldots (22)$$

for mixed-wet drainage relative permeability to water, and, from Eqs. 12 and 14,

$$k_{rod} = \frac{p_{cwd}k_{ro,wwd} - p_{cod}k_{ro,owd}}{p_{cwd} - p_{cod}} \quad \ldots\ldots\ldots\ldots\ldots\ldots\ldots\ldots (23)$$

for mixed-wet drainage relative permeability to oil, with unity endpoint values. The expressions have to be adjusted by the endpoint values k^0_{rw} and k^0_{ro} at the residual saturations S_{oR} and S_{wR}, respectively. With subscript i replacing d, the equations are also valid for the imbibition process. In these expressions, the a- and c-parameters all have the same values as in the corresponding capillary pressure correlation. The tortuosity exponents m, however, are additional parameters just for the relative permeability functions.

The wettability is no longer given by a single number, an index, but is a wettability function, $(p_{cwd}+p_{cod})/(p_{cwd}-p_{cod})$, exemplified in **Fig. 8.** It approaches completely water-wet conditions (+1 or ww) in the limit of S_{wR} and completely oil-wet conditions (−1 or ow) in the limit $1-S_{oR}$. There is one wettability function for drainage and another for imbibition. We have also tried other weighting procedures (e.g., p_c^2-averaging), but p_c-averaging seems to be the best alternative.

Primary drainage relative permeabilities may be modeled by $k_{rw,wwd}$ and $k^0_{ro}\cdot k_{ro,wwd}$, with a_{wd} from a fit of the primary drainage capillary pressure, if such data are available. The default value of the tortuosity exponent m is the Burdine-value of 2.

Matching Measured Data. We have tested the relative permeability correlation on a consistent set of capillary-pressure and relative-permeability measurements published by Honarpour *et al.*[10] The as and cs are found by curve-fitting the capillary pressure data, **Fig. 9,** and with all ms equal to the default value of 2, we can predict the relative permeability functions. As an estimate of the endpoint value k^0_{rw}, values from neighboring core plugs or from analogous porous media may be used. If no such information is available, it seems reasonable to assume that the bounding imbibition relative permeability at S_{oR} should be greater or equal to the primary drainage curve.[33] If no primary drainage data are known, an approximate value is $k_{rw,wwd}$ with a_{wd} from the capillary pressure match. The estimate of k^0_{rw} then is $k_{rw,wwd}(S_{oR})$.

The first set of estimated relative permeability curves from the capillary pressure data may deviate from the measured relative permeability data, if available. Adjustments of m, k^0_{ro}, and k^0_{rw} may be needed. We used the Solver function of the Microsoft Excel spreadsheet to curve-fit relative permeability data by minimizing the sum of errors squared between the calculated and measured values. Each squared error was weighted by the inverse k_r-value. The fit is shown in **Figs. 10 through 12.** The fitted curves in Figs. 11 and 12 match the data better at low relative permeability because the squared errors are weighted by the inverse. In **Fig. 13**

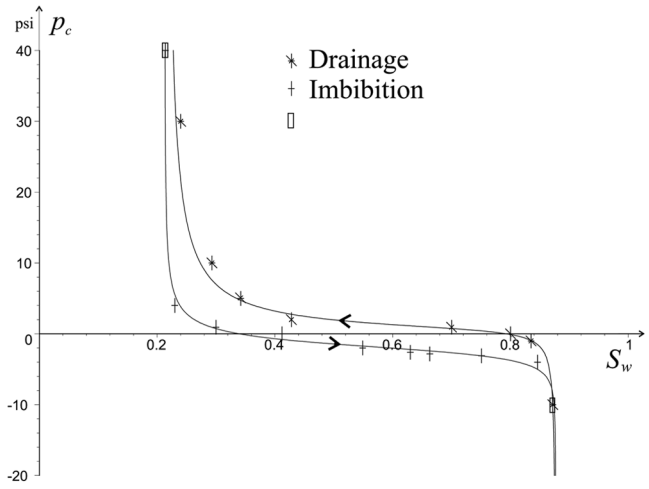

Fig. 9—Capillary pressure correlation fitted to data measured by Honarpour *et al.*[10]

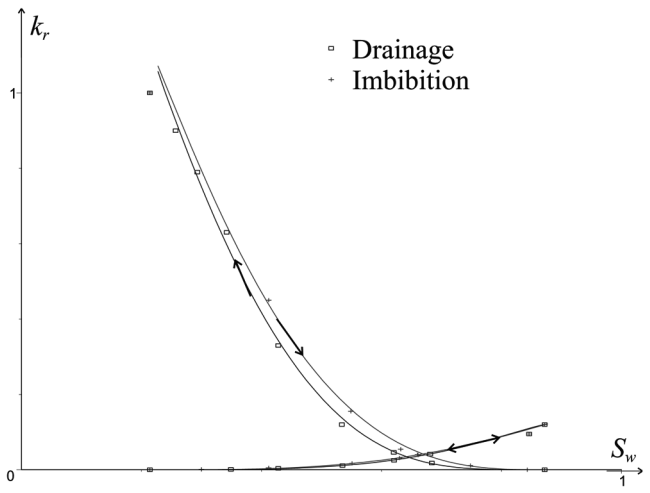

Fig. 10—Relative permeability correlation fitted to measured data by Honarpour *et al.*[10]

are shown the measured oil drainage data, together with the fitted k_{rod}-curve and the limiting $k_{ro,wwd}$- and $k_{ro,owd}$-curves for oil- and water-wet systems, respectively.

Relative Permeability Hysteresis Logic

Relative permeability hysteresis has been considered of significance only between the primary drainage and the imbibition curves. Many measurements have been made of these processes.[7,26,28,34] Hysteresis between secondary drainage and imbibition curves has also been recognized by several authors,[4,10,25,29,30,32] but there are few published data on relative permeability scanning curves. The most extensive set of such data is that of Braun and Holland,[4] who used a pseudosteady-state method. A series of oil relative permeability scanning curves were measured, originating on the bounding imbibition or bounding drainage curve. These measurements are illustrated in **Figs. 14 and 15**, modeled by the hysteresis logic described below:

- The suite of oil drainage scanning curves that originate on the bounding imbibition curve scan back toward the point (S_{wR}, k^0_{rw}), the last reversal point, approaching the bounding drainage curve (Fig. 14).
- The suite of oil imbibition scanning curves spawned on the bounding drainage curve scan back toward the point (S_{oR},0), approaching the bounding imbition curve (Fig. 15).

These observations are similar to those of Morrow and Harris[21] for the capillary-pressure scanning curves. The data[4] also show that the scanning loops are closed. A scanning curve from $S_w[j]$ will scan back to $S_w[j-1]$ and form a closed loop. Unless interrupted by another reversal, the process will shunt to the $[j-2]$ curve, as if the $[j-1]$ reversal never had occurred, as illustrated in **Figs. 16 and 17.**

Braun and Holland[4] find the relative permeability scanning curves to be reversible. The saturation intervals of the scanning loops are so small, however, that hysteresis, if present, would experimentally be difficult to detect (e.g., the modeled results in Figs. 16 and 17 which closely resemble some of the measured cases). Also, we expect both water- and oil-relative permeability in a mixed-wet system to show similar hysteretic behavior, and that oil relative permeability in an oil-wet system will exhibit negligible hysteresis, as does water relative permeability in a water-wet system.

Procedure. The suggested procedure for modeling relative permeability scanning curves is consistent with the procedure for modeling the capillary pressure scanning curves. The same convention for labels is used: all properties of the jth scanning curve are labeled by $[j]$. The relative permeability functions are denoted by $k_{rod}[j]$, $k_{rwd}[j]$, $k_{roi}[j]$, and $k_{rwi}[j]$, and saturation reversals occur at $S_w[j]$. For imbibition curves, defined by increasing water saturation, all properties are odd-numbered, and they are even-numbered for drainage curves.

The first imbibition relative permeability scanning curves, $k_{roi}[1]$ and $k_{rwi}[1]$, start on the primary drainage curve, labeled [0], at $S_w[1]$ and scan toward a residual oil saturation $S_{oR}[1]$ as deter-

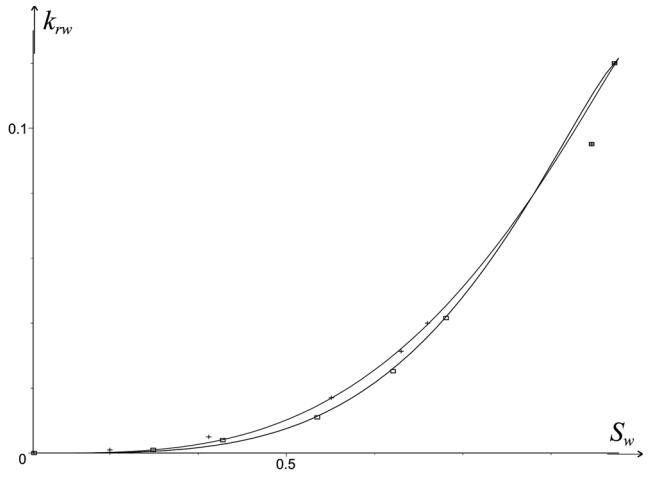

Fig. 11—Detail of Fig. 10, water relative permeability.

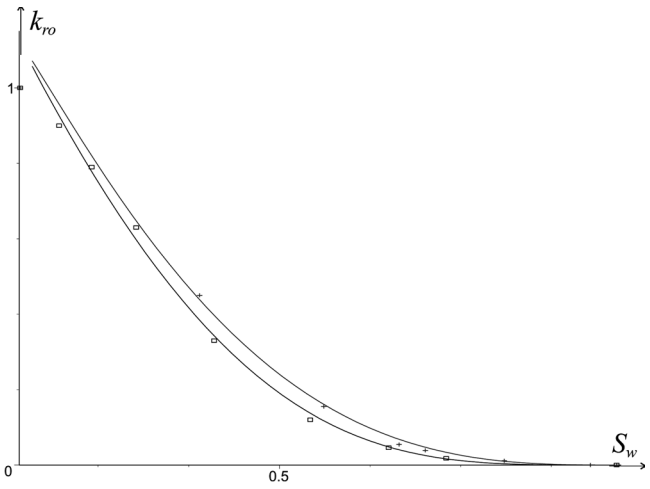

Fig. 12—Detail of Fig. 10, oil relative permeability.

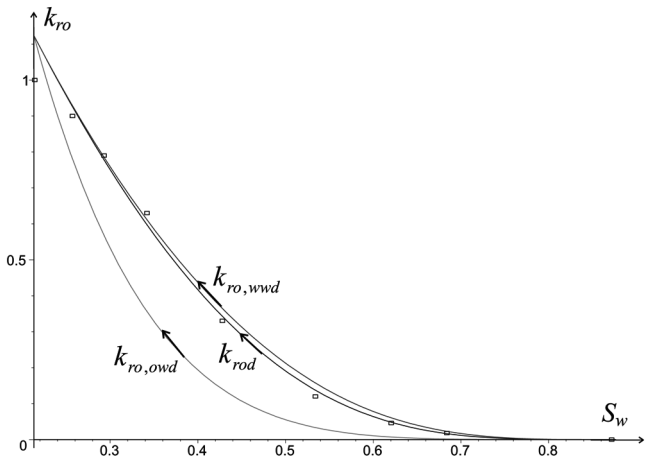

Fig. 13—Limiting and predicted drainage oil-relative permeability curves, together with measured data.

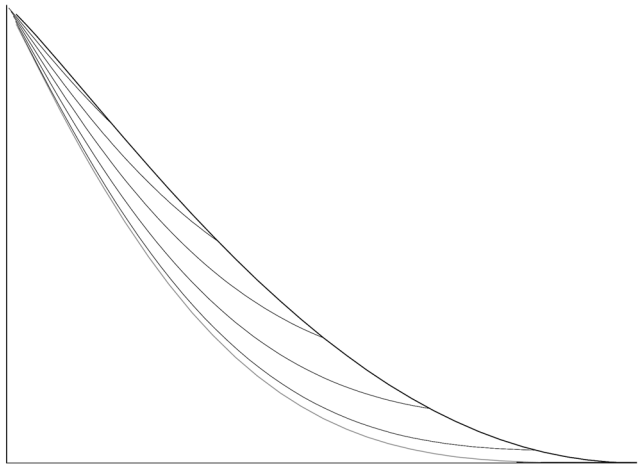

Fig. 14—Modeled oil-drainage scanning curves originating on the bounding imbibition curve.

mined by Eq. 6. The normalized saturations S_{no} and S_{nw} are now generalized and redefined to

$$S_{nw} = \frac{S_w - S_{wR}}{1 - S_{wR} - S_{oR}[1]} \quad \ldots\ldots\ldots\ldots\ldots\ldots\ldots\ldots\ldots\ldots (24)$$

and

$$S_{no} = \frac{S_o - S_{oR}[1]}{1 - S_{wR} - S_{oR}[1]}. \quad \ldots\ldots\ldots\ldots\ldots\ldots\ldots\ldots\ldots\ldots (25)$$

If the first reversal from the primary drainage curve occurs at irreducible water saturation (i.e., $S_w[1] = S_{wR}$), then $S_{oR}[1] = S_{oR}$ and S_{nw} and S_{no} revert to their previous definitions. With normalized saturations from Eqs. 24 and 25, the Corey-type relative permeabilities for completely oil- or water-wet rock are still given by the expressions in Eqs. 11 through 14.

The wettability weighting scheme, Eqs. 22 and 23, also needs to be generalized to include cases in which the first saturation reversal from the primary drainage curve occurs before the process reaches S_{wR} (i.e., if $S_w[1] > S_{wR}$). In the expression for p_{coi}, the imbibition oil-branch weight of Eq. 10, we replace S_{oR} by $S_{oR}[1]$ and denote the result by p^1_{coi}. And likewise, in the expression for p_{cod}, we replace S_{oR} by $S_{oR}[1]$ and denote the result by p^1_{cod}, the oil-branch weight for a second (drainage) reversal from $S_{oR}[1]$. No changes are made in the water-branch weights (Eq. 9). With these adjusted weights, the scanning relative permeability curves will be mixed-wet near $S_w[1]$ and completely oil-wet at $S_{oR}[1]$, which seems reasonable. If we assume that primary drainage occurs at water-wet conditions, the porous medium will be subject to aging before any reversal occurs. It is therefore perhaps reasonable with a discontinuity in wettability at $S_w[1]$.

The mixed-wet relative permeability functions of the bounding scanning processes originating at $S_w[1]$ that correspond to the global bounding curves of Eqs. 22 and 23 are denoted by k^1_{rwi}, k^1_{rwd}, k^1_{roi}, and k^1_{rod} and given by

$$k^1_{rwi}(S_w) = \frac{p_{cwi} \cdot k_{rw,wwi} - p^1_{coi} \cdot k_{rw,owi}}{p_{cwi} - p^1_{coi}}, \quad \ldots\ldots\ldots\ldots\ldots (26)$$

$$k^1_{rwd}(S_w) = \frac{p_{cwd} \cdot k_{rw,wwd} - p^1_{cod} \cdot k_{rw,owd}}{p_{cwd} - p^1_{cod}}, \quad \ldots\ldots\ldots\ldots\ldots (27)$$

$$k^1_{roi}(S_w) = \frac{p_{cwi} \cdot k_{ro,wwi} - p^1_{coi} \cdot k_{ro,owi}}{p_{cwi} - p^1_{coi}}, \quad \ldots\ldots\ldots\ldots\ldots (28)$$

and

$$k^1_{rod}(S_w) = \frac{p_{cwd} \cdot k_{ro,wwd} - p^1_{cod} \cdot k_{ro,owd}}{p_{cwd} - p^1_{cod}}. \quad \ldots\ldots\ldots\ldots\ldots (29)$$

We now stipulate that within the bounding scanning loop initiated at the reversal $S_w[1]$, all relative permeability scanning curves may be represented by a simple linear expression of the corresponding relative permeability function in Eqs. 26 through 29. That is, for

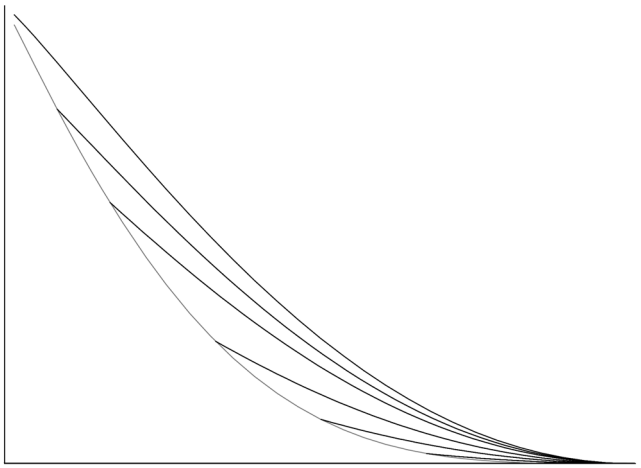

Fig. 15—Modeled oil-imbibition scanning curves originating on the bounding drainage curve.

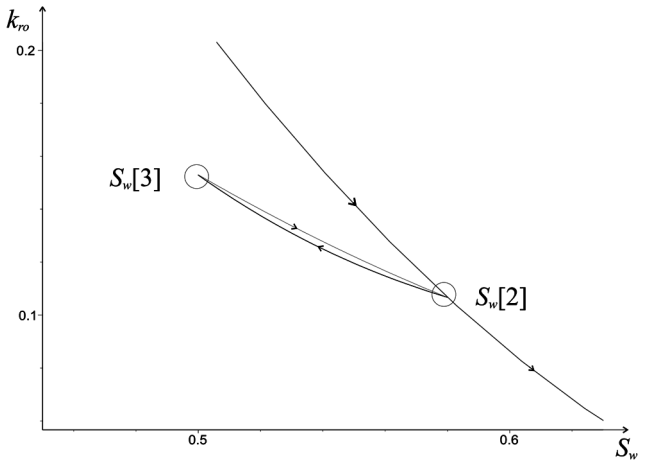

Fig. 16—Modeled closed scanning loop originating on bounding imbibition curve.

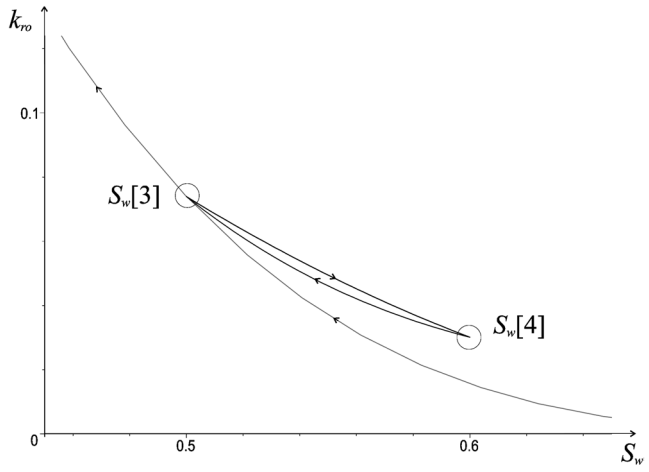

Fig. 17—Modeled closed scanning loop originating on the bounding drainage curve.

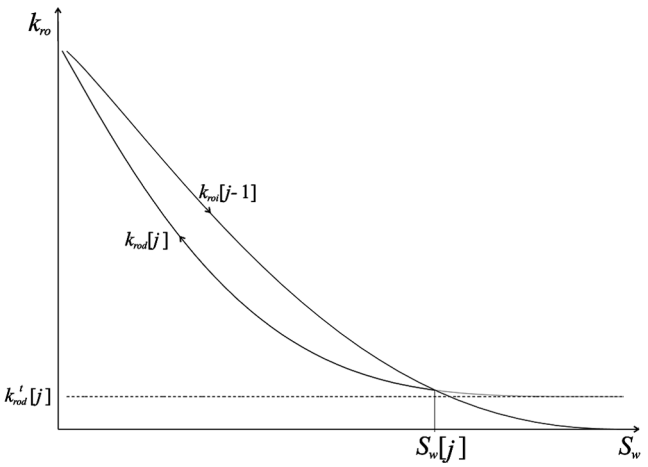

Fig. 18—Drainage scanning curve originating on bounding imbibition curve. Horizontal line represents the value of $k^t_{rod}[j]$.

imbibition processes following an odd-numbered reversal, starting at $j=1$,

$$k_{rwi}[j](S_w) = k^0_{rwi}[j] \cdot k^1_{rwi}(S_w) + k^t_{rwi}[j], \quad \ldots\ldots\ldots\ldots\ldots\ldots (30)$$

$$k_{roi}[j](S_w) = k^0_{roi}[j] \cdot k^1_{roi}(S_w) + k^t_{roi}[j], \quad \ldots\ldots\ldots\ldots\ldots\ldots (31)$$

and for drainage processes following an even-numbered reversal, starting at $j=2$,

$$k_{rwd}[j](S_w) = k^0_{rwd}[j] \cdot k^1_{rwd}(S_w) + k^t_{rwd}[j], \quad \ldots\ldots\ldots\ldots\ldots\ldots (32)$$

$$k_{rod}[j](S_w) = k^0_{rod}[j] \cdot k^1_{rod}(S_w) + k^t_{rod}[j]. \quad \ldots\ldots\ldots\ldots\ldots\ldots (33)$$

In these expressions, $k^0_{rpa}[j]$ and $k^t_{rpa}[j]$ are constants for a given j. Subscript p denotes phase and is equal to w or o, and α denotes process type and is equal to i or d. The constant $k^t_{rpa}[j]$ is a fictitious threshold relative permeability value—the scanning relative permeability value at endpoint saturation of the bounding scanning loop. **Fig. 18** illustrates the $k^t_{rod}[j]$-value for a drainage reversal from an imbibition curve. It is the vertical shift of the relative permeability function $k^1_{rod}(S_w)$ which has been scaled by the factor $k^0_{rod}[j]$. Each of Eqs. 30 through 33 therefore has two constants, $k^0_{rpa}[j]$and $k^t_{rpa}[j]$. They are determined by the two equations that enforce closed scanning loops (i.e., by requiring that the two scanning curves have the same relative permeability values at the start and end of the loop).

First Reversal. A first saturation reversal at $S_w[1]$ on the primary drainage curve labeled [0] spawns an imbibition process labeled [1], which scans toward $S_{oR}[1]$ **(Figs. 19 and 20).** For the case when $S_w[1]=S_{wR}$, the imbibition scanning curve is the global bounding imbibition curve, and $S_{oR}[1]$ is equal to S_{oR}. Consistent with the hysteresis logic for the capillary pressure curves, $S_{oR}[1]$ is determined by Land's[34] trapping relation (Eq. 6).

Oil Relative Permeability. At the reversal point $S_w[1]$, the relative permeability value on the imbibition scanning curve is equal to that of the primary drainage curve,

$$k_{roi}[1](S_w[1]) = k_{rod}[0](S_w[1]), \quad \ldots\ldots\ldots\ldots\ldots\ldots (34)$$

and at the other endpoint, at $S_{oR}[1]$, by definition, $k_{roi}[1](S_{oR}[1])=0$. At this endpoint, $S_{nw}=1$ and $S_{no}=0$, from Eqs. 24 and 25; from Eq. 12, $k_{ro,wwi}=0$, and from Eq. 14, $k_{ro,owi}=0$. Therefore, from Eq. 28, $k^1_{roi}[j](S_{oR}[1])=0$, and finally, from Eq. 31, the constant $k^t_{roi}[1]=0$. Therefore, Eq. 34 is solved with respect to the constant $k^0_{roi}[1]$.

Water Relative Permeability. The water relative permeability curve scans from the reversal point on the primary drainage curve, which requires that $k_{rwi}[1](S_w[1])=k_{rwd}[0](S_w[1])$, as in Eq. 34. At the other endpoint, at $S_{oR}[1]$, we have that $k_{rwi}[1](S_{oR}[1])=k^0_{rw}(S_{oR}[1])$, where k^0_{rw} is a certain function of the residual oil saturation (cf. discussion in Standing's report[2]). To our knowledge, no study has been published on this relation. We have therefore chosen to use linear interpolation between $k_{rwi}(S_{oR})$, endpoint for the global bounding imbibition curve, and $k_{rwd}[0](S_w=1)=1$

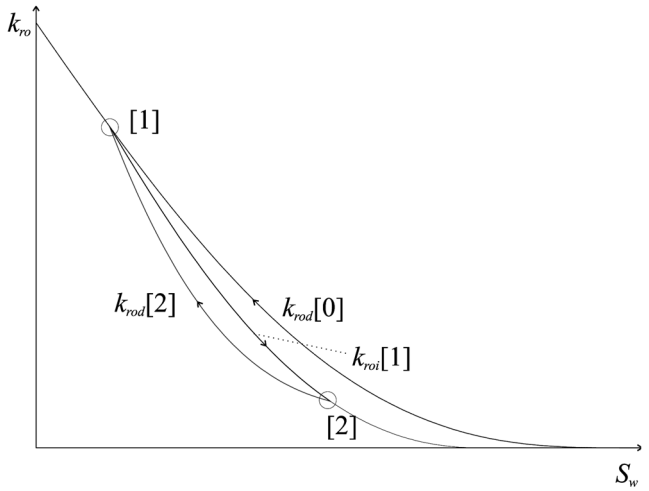

Fig. 19—Oil relative-permeability scanning curves originating from reversal [1] on the primary drainage curve, $k_{rod}[0]$.

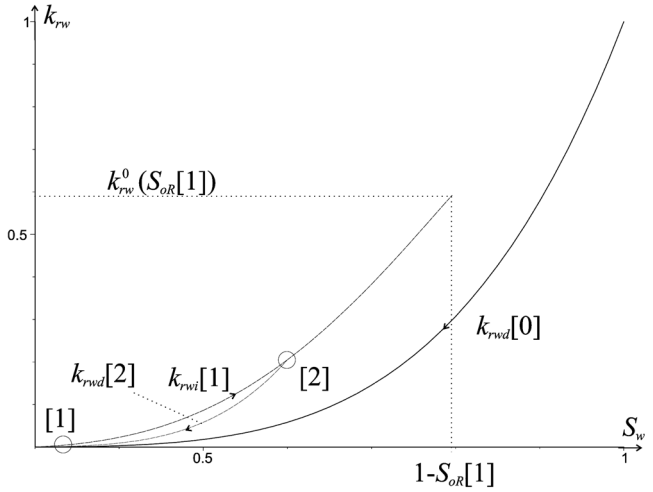

Fig. 20—Water relative-permeability scanning curves originating from reversal [1] on the primary drainage curve $k_{rwd}[0]$.

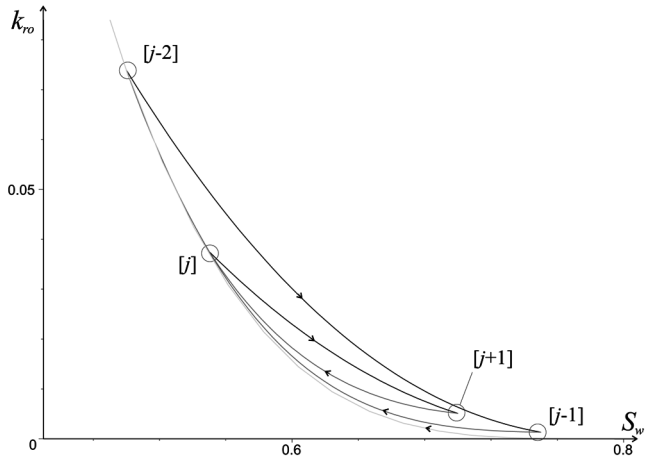

Fig. 21—Modeled scanning loops for oil relative permeability.

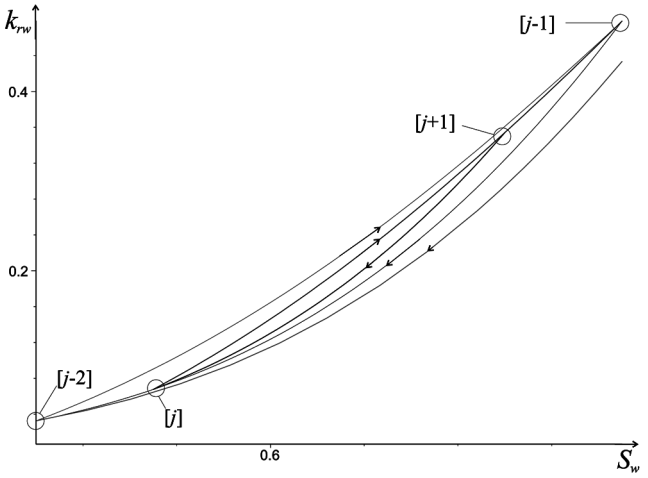

Fig. 22—Modeled scanning loops for water relative permeability.

to estimate $k^0_{rw}(S_{oR}[1])$. The same method is used by Killough[14] and Eikje *et al.*[32]

Second Reversal. A second reversal will start a drainage process labeled [2] from the reversal saturation $S_w[2]$, aiming back at $S_w[1]$.

Oil Relative Permeability. To have closed scanning loops, oil relative permeabilities of the two scanning curves have to be equal at the new reversal point, $k_{rod}[2](S_w[2]) = k_{roi}[1](S_w[2])$, and at the previous reversal point labeled [1], $k_{rod}[2](S_w[1]) = k_{roi}[1](S_w[1])$. The $k_{rod}[2]$-curve is shown in Fig. 19.

Water Relative Permeability. The corresponding equations for the water relative permeability scanning curve are $k_{rwd}[2](S_w[2]) = k_{rwi}[1](S_w[2])$ and $k_{rwd}[2](S_w[1]) = k_{rwi}[1](S_w[1])$, and the $k_{rwd}[2]$-curve is shown in Fig. 20. The drainage process [2] will scan back to reversal point [1] and subsequently follow the primary drainage curve, labeled [0]. Any new reversal will thereafter be equivalent to a first reversal. A third reversal may, however, occur before the process reaches back to reversal point [1].

Third Reversal. A third reversal before the process reaches back to [1] will start an imbibition process from saturation reversal $S_w[3]$ scanning back to $S_w[2]$. If this process, labeled [3], passes through reversal point [2], it will retrace process [1].

Oil Relative Permeability. The third oil-imbibition relative-permeability curve scans from $k_{roi}[3](S_w[3]) = k_{rod}[2](S_w[3])$ at the new reversal point, to $k_{roi}[3](S_w[2]) = k_{rod}[2](S_w[2])$ at the previous reversal point.

Water Relative Permeability. The corresponding equations for the water relative-permeability scanning curve are $k_{rwi}[3](S_w[3]) = k_{rwd}[2](S_w[3])$ and $k_{rwi}[3](S_w[2]) = k_{rwd}[2](S_w[2])$.

General Reversals. The methodology for creating scanning curves may easily be generalized from the observations that they form closed loops (i.e., a process with reversal at $S_w[j]$ will return to $S_w[j-1]$). **Figs. 21 and 22** show one closed scanning loop [*j*]–[*j*+1]–[*j*], inside of an outer scanning loop [*j*–2]–[*j*–1]–[*j*–2]. The outer loop has an imbibition process from [*j*–2] to [*j*–1], where the saturation change is reversed. The drainage curve scans back to [*j*–2] but is interrupted by the inner loop's imbibition process from [*j*] to [*j*–1]. This process is interrupted at [*j*+1], with a drainage scan back to [*j*]. Continued drainage after reaching [*j*] causes tracing of the drainage scanning curve from [*j*–1] to [*j*–2].

Imbibition Oil Relative Permeability. The general oil imbibition relative permeability curve scans from

$$k_{roi}[j](S_w[j]) = k_{rod}[j-1](S_w[j]) \quad \ldots\ldots\ldots\ldots\ldots\ldots\ldots (35)$$

at reversal point [*j*] to

$$k_{roi}[j](S_w[j-1]) = k_{rod}[j-1](S_w[j-1]) \quad \ldots\ldots\ldots\ldots\ldots\ldots\ldots (36)$$

at reversal point [*j*–1].

The two unknown parameters $k^0_{roi}[j]$ and $k^t_{roi}[j]$ of imbibition scanning curve labeled [*j*] may be expressed by

$$k^0_{roi}[j] = k^0_{rod}[j-1]\left\{\frac{k^1_{rod}(S_w[j]) - k^1_{rod}(S_w[j-1])}{k^1_{roi}(S_w[j]) - k^1_{roi}(S_w[j-1])}\right\}, \quad \ldots\ldots\ldots (37)$$

and

$$k^t_{roi}[j] = k^t_{rod}[j-1] + k^0_{rod}[j-1]\cdot k^1_{rod}(S_w[j]) - k^0_{roi}[j]\cdot k^1_{roi}(S_w[j]), \quad \ldots\ldots\ldots\ldots\ldots\ldots\ldots (38)$$

when Eqs. 31 and 33 are introduced in Eqs. 35 and 36.

Imbibition Water Relative Permeability. The general equations for water relative permeability curves are $k_{rwi}[j](S_w[j]) = k_{rwd}[j-1](S_w[j])$ at reversal point [*j*] to $k_{rwi}[j](S_w[j-1]) = k_{rwd}[j-1](S_w[j-1])$ at reversal point [*j*–1], and

$$k^0_{rwi}[j] = k^0_{rwd}[j-1]\left\{\frac{k^1_{rwd}(S_w[j]) - k^1_{rwd}(S_w[j-1])}{k^1_{rwi}(S_w[j]) - k^1_{rwi}(S_w[j-1])}\right\} \quad \ldots\ldots\ldots (39)$$

and

$$k^t_{rwi}[j] = k^t_{rwd}[j-1] + k^0_{rwd}[j-1]\cdot k^1_{rwd}(S_w[j]) - k^0_{rwi}[j]\cdot k^1_{rwi}(S_w[j]), \quad \ldots\ldots\ldots\ldots\ldots\ldots\ldots (40)$$

If the *i*s and *d*s are swapped, the equations are equally valid for general drainage scanning curves.

Discussion

Validation of Hysteresis Logic. The hysteresis model has to be checked against measured data. It has been designed, however, to qualitatively honor the characteristic features of the measurements of Braun and Holland,[4] who did not measure capillary pressure. The lack of consistent capillary pressure and relative permeability measurements on the same core sample makes it difficult to determine the *a*s and *c*s of the capillary pressure correlation. A series of measurements for checking the model should include the capillary pressure and relative permeability of the bounding hysteresis loop and a variety of scanning curves and loops, possibly measured by a technique similar to that of Honarpour *et al.*[10]

Figs.16 and 17 show that modeled scanning loops exhibit negligible hysteresis when $\Delta S_w = S_w[j] - S_w[j-1]$ is small, in accordance with the observations of Braun and Holland.[4] Furthermore, modeled scanning curves originating on the bounding imbibition or drainage curve all scan back to the residual phase saturation, Figs. 14 and 15. This is also in agreement with the observations by Braun and Holland.

No attempt has been made to model the measured scanning curves of Braun and Holland[4] with capillary pressure parameters *a* and *c* determined from matching their measured bounding relative permeability curves. This probably would not give any definite

arguments to keep or reject the model. As discussed in detail by Lohne,[35] the starting points of the scanning curves (i.e., the saturation reversal points of Braun and Holland) are not properly located on the bounding hysteresis loop, which was measured first.

Scaling. Kriebernegg and Heinemann[36] chose to scale the whole bounding drainage and imbibition curves to model the scanning curves. We believe that scaling and vertical shifting of the k^1_{rpa}-curves is more reasonable. Then, for example, if there is no hysteresis between the bounding imbibition and drainage curves, a drainage scanning curve from the bounding imbibition curve will exhibit no hysteresis, regardless of size of the saturation interval ($S_w[j]-S_{wR}$). Otherwise, if the whole bounding drainage curve is scaled to fit between $S_w[j]$ and S_{wR}, the hysteresis becomes more pronounced as the saturation interval decreases.

Implementation. Eigestad and Larsen[37] have implemented the capillary-pressure and relative-permeability hysteresis models described here in a fully implicit numerical reservoir model. Several simulation runs are reported, and it is discussed how the rate of rise of the free water table affects the shape of the capillary transition zone. The results are compared with those from a commercial reservoir simulator, which employs the Killough hysteresis scheme.

Conclusions

1. A new two-phase model for mixed-wet relative permeability curves is developed and covers primary drainage, imbibition, and secondary drainage. The correlation is the sum of two Corey-type relative permeability expressions, weighted with the branches of the capillary pressure correlation.
2. The two Corey expressions represent completely water- and oil-wet systems. Through the weighting, the wettability is made saturation-dependent.
3. The relative permeability correlation is integrated and bundled with the capillary-pressure correlation.
4. In addition to the capillary pressure, an extra set of parameters are introduced to improve the match of relative permeability data (i.e., tortuosity exponents).
5. Curve fitting a consistent set of capillary pressure and relative permeability data gives good results.
6. An associated hysteresis logic treats scanning curves from primary drainage and inside the bounding hysteresis loop. Modeled hysteresis curves exhibit the same behavior as that observed by Braun and Holland.
7. The hysteresis logic is a unified procedure for relative-permeability and capillary-pressure functions.
8. Further validation should be made from consistent and simultaneously measured datasets of capillary-pressure and relative-permeability scanning curves.
9. A systematic study of the tortuosity exponents and endpoint relative permeability values is needed.

Nomenclature

a = constant, dimensionless
c = constant, psi, bar or mbar
C = Land's trapping constant, dimensionless
$[j]$ = label, saturation reversal number j and the subsequent scanning curve
j = saturation reversal counter
k_r = relative permeability, dimensionless
m = tortuosity exponent, dimensionless
p = pressure, psi, bar or mbar
S = saturation

Subscripts

c = capillary
d = drainage
i = imbibition or initial
n = normalized
o = oil
ow = oil-wet
p = phase (o or w)
r = relative
R = residual
w = water
ww = water-wet
α = process (d for drainage or i for imbibition)
0 = zero point ($p_c = 0$)

Superscripts

t = threshold
0 = endpoint
1 = associated with bounding scanning curves of first reversal at $S_w[1]$

Acknowledgments

We thank E.M. Braun and M.M. Honarpour for direct access to unique data sets, and J.A. Larsen for constructive discussions. We would also like to thank Den norske stats oljeselskap a.s. (Statoil) for support and permission to publish the paper.

References

1. Skjaeveland, S.M. *et al.:* "Capillary Pressure Correlation for Mixed-Wet Reservoirs," *SPEREE* (February 2000) 60.
2. Standing, M.B.: *Notes on Relative Permeability Relationships, Proc.,* U. of Trondheim, Norway (1975).
3. Burdine, N.T.: "Relative Permeability Calculations From Pore Size Distribution Data," *Trans.,* AIME (1953) **198,** 71.
4. Braun, E.M. and Holland, R.F.: "Relative Permeability Hysteresis: Laboratory Measurements and a Conceptual Model," *SPERE* (August 1995) 222.
5. Huang, D.D., Honarpour, M.M., and Al-Hussainy, R.: "An Improved Model for Relative Permeability and Capillary Pressure Incorporating Wettability," paper presented at the 1997 Society of Core Analysts International Symposium, Calgary, 7–10 September.
6. Lenhard, R.J. and Oostrom M.: "A Parametric Model for Predicting Relative Permeability-Saturation-Capillary Pressure Relationships of Oil–Water Systems in Porous Media with Mixed Wettability," *Transport in Porous Media* (1998) **31,** 109.
7. Osoba, J.S. *et al.:* "Laboratory Measurements of Relative Permeability," *Trans.,* AIME (1951) **192,** 47.
8. Hagoort, J.: "Measurements of Relative Permeability for Computer Modeling/Reservoir Simulation," *Oil & Gas J.* (February 1984) 62.
9. Chierici, G.L.: "Novel Relations for Drainage and Imbibition Relative Permeabilities," *SPEJ* (September 1975) 275.
10. Honarpour, M.M., Huang, D.D., and Al-Hussainy, R.: "Simultaneous Measurements of Relative Permeability, Capillary Pressure, and Electrical Resistivity With Microwave System for Saturation Monitoring," *SPEJ* (September 1996) 283.
11. McDougall, S.R. and Sorbie, K.S.: "The Impact of Wettability on Waterflooding: Pore-Scale Simulation," *SPERE* (August 1995) 208.
12. Anderson, W.G.: "Wettability Litterature Survey–Part 5: Effect of Wettability on Relative Permeability," *JPT* (November 1987) 1453.
13. Guzmán, R.E. and Fayers, F.J.: "Mathematical Properties of Three-Phase Flow Equations," *SPEJ* (September 1997) 291.
14. Killough, J.E.: "Reservoir Simulation With History-Dependent Saturation Functions," *SPEJ* (February 1976) 37; *Trans.*, AIME, **261.**
15. Laroche, C., Vizika, O., and Kalaydjian, F.: "Network Modeling To Predict the Effect of Wettability Heterogeneities on Multiphase Flow," paper SPE 56674 presented at the 1999 SPE Annual Technical Conference and Exhibition, Houston, 3–6 October.
16. Larsen, J.A. and Skauge, A.: "Simulation of the Immiscible WAG Process Using Cycle-Dependent Three-Phase Relative Permeabilities," paper SPE 56475 presented at the 1999 SPE Annual Technical Conference and Exhibition, Houston, 3–6 October.
17. Moulu, J.-C. *et al.:* "A New Three-Phase Relative Permeability Model for Various Wettability Conditions," paper SPE 56477 presented at the 1999 SPE Annual Technical Conference and Exhibition, Houston, 3–6 October.
18. Alpak, F.O., Lake, L.W., and Embid, S.M.: "Validation of a Modified Carman-Kozeny Equation To Model Two-Phase Relative Permeabili-

ties," paper SPE 56479 presented at the 1999 SPE Annual Technical Conference and Exhibition, Houston, 3–6 October.
19. Brooks, R.H. and Corey, A.T.: "Hydraulic Properties of Porous Media," Hydraulic Paper No. 3, Colorado State U., Fort Collins (1964).
20. Brooks, R.H. and Corey, A.T.: "Properties of Porous Media Affecting Fluid Flow," *J. of the Irrigation and Drainage Division, Proc. of ASCE,* (1966) **92**, No. IR2, 61.
21. Morrow, N.R. and Harris, C.C.: "Capillary Equilibrium in Porous Materials," *SPEJ* (March 1965) 15.
22. Wardlaw, N.C. and Taylor, R.P.: "Mercury Capillary Pressure Curves and the Interpretation of Pore Structure and Capillary Behaviour in Reservoir Rocks," *Bull. Can. Pet. Geo.* (June 1976) **24,** No. 2, 225.
23. Hammervold, W.L. *et al.:* "Capillary Pressure Scanning Curves by the Micropore Membrane Technique," *J. Pet. Sci. & Eng.* (1998) **20,** 253.
24. Topp, G.C. and Miller, E.E.: "Hysteretic Moisture Characteristics and Hydraulic Conductivities for Glass-Bead Media," *Soil Sci. Soc. Amer. Proc.* (1966) **30,** 156.
25. Colonna, J., Brissaud, F., and Millet, J.L.: "Evolution of Capillarity and Relative Permeability Hysteresis," *SPEJ* (February 1972) 28; *Trans.,* AIME, **253.**
26. Land, C.S.: "Calculation of Imbibition Relative Permeability for Two- and Three Phase Flow From Rock Properties," *SPEJ* (June 1968) 149; *Trans.,* AIME, **243.**
27. Amyx, J.W., Bass, D.M., and Whiting, R.T.: *Petroleum Reservoir Engineering,* McGraw-Hill, New York City (1960) 133–210.
28. Geffen, T.M. *et al.:* "Experimental Investigation of Factors Affecting Laboratory Relative Permeability Measurements," *Trans*., AIME (1951) **192,** 99.
29. Evrenos, A.I. and Comer, A.G.: "Numerical Simulation of Hysteretic Flow in Porous Media," paper SPE 2693 presented at the 1969 SPE Annual Fall Meeting, Denver, 28 September–1 October.
30. Braun, E.M. and Blackwell, R.J.: "A Steady-State Technique for Measuring Oil-Water Relative Permeability Curves at Reservoir Conditions," paper SPE 10155 presented at the 1981 SPE Annual Technical Conference and Exhibition, San Antonio, Texas, 5–7 October.
31. Honarpour, M., Koederitz, L., and Harvey, A.H.: *Relative Permeability of Petroleum Reservoir*s, CRC Press, Inc., New York City (1986).
32. Eikje, E. *et al.:* "Relative Permeability Hysteresis in Micellar Flooding," *J. Pet. Sci. Eng.* (1992) **7,** No. 1–2, 91.
33. Larsen, J.A.: "Evaluation of Transport Properties for Immiscible Flow in Porous Media," PhD dissertation, U. Bergen, Bergen, Norway (1997).
34. Land, C.S.: "Comparison of Calculated With Experimental Imbibition Relative Permeability," *SPEJ* (December 1971); *Trans*., AIME, **251.**
35. Lohne, A.: "Hysteresis in Two- and Three-Phase Flow in Porous Medium," MS thesis, Stavanger College, Stavanger, Norway (1998).
36. Kriebernegg, M. and Heinemann, Z.: "A New Model for History Dependent Saturation Functions in Reservoir Simulation," paper presented at the 1996 European Conference on the Mathematics of Oil Recovery, Leoben, Austria, 3–6 September.
37. Eigestad, G.T. and Larsen, J.A.: "Numerical Modeling of Capillary Transition Zones," paper SPE 64374 presented at the 2000 SPE Asia Pacific Oil and Gas Conference and Exhibition, Brisbane, Australia, 16–18 October.

SI Metric Conversion Factors

bar × 1.0*	E+05	= Pa
psi × 6.894 757	E+00	= kPa

*Conversion factor is exact.

Arnfinn Kjosavik is a reservoir engineer with Statoil. e-mail: arkjo@statoil.com. He holds BS and MS degrees in petroleum engineering from Stavanger U. College. **Jon Knut Ringen** is a technical adviser in Statoil. e-mail: jkr@statoil.com. He holds an MS degree in physical chemistry from the U. of Bergen. **Svein M. Skjaeveland** is a professor of petroleum engineering at Stavanger U. College. e-mail: s-skj@ux.his.no. He holds a PhD degree in physics from the Norwegian U. of Science and Technology and in petroleum engineering from Texas A&M U.